Predicting Non-Stationary and Stochastic Activation of Saddle-Node Bifurcation

Jinki Kim[1]
Department of Mechanical Engineering,
University of Michigan,
Ann Arbor, MI 48109
e-mail: jinkikim@umich.edu

R. L. Harne
Department of Mechanical and
Aerospace Engineering,
The Ohio State University,
Columbus, OH 43210

K. W. Wang
Department of Mechanical Engineering,
University of Michigan,
Ann Arbor, MI 48109

Accurately predicting the onset of large behavioral deviations associated with saddle-node bifurcations is imperative in a broad range of sciences and for a wide variety of purposes, including ecological assessment, signal amplification, and microscale mass sensing. In many such practices, noise and non-stationarity are unavoidable and ever-present influences. As a result, it is critical to simultaneously account for these two factors toward the estimation of parameters that may induce sudden bifurcations. Here, a new analytical formulation is presented to accurately determine the probable time at which a system undergoes an escape event as governing parameters are swept toward a saddle-node bifurcation point in the presence of noise. The double-well Duffing oscillator serves as the archetype system of interest since it possesses a dynamic saddle-node bifurcation. The stochastic normal form of the saddle-node bifurcation is derived from the governing equation of this oscillator to formulate the probability distribution of escape events. Non-stationarity is accounted for using a time-dependent bifurcation parameter in the stochastic normal form. Then, the mean escape time is approximated from the probability density function (PDF) to yield a straightforward means to estimate the point of bifurcation. Experiments conducted using a double-well Duffing analog circuit verifies that the analytical approximations provide faithful estimation of the critical parameters that lead to the non-stationary and noise-activated saddle-node bifurcation.
[DOI: 10.1115/1.4034128]

Keywords: non-stationary and stochastic saddle-node bifurcation, normal form, double-well Duffing oscillator analog circuit

1 Introduction and Motivation

The saddle-node bifurcation is the focus of a substantial body of research, since it is one of the most commonly encountered phenomena that induce sudden, drastic changes in the global behavior of systems. It is well documented that activation of the saddle-node bifurcation is strongly influenced by non-deterministic and non-stationary factors. For example, stochastic processes may result in noise-activated saddle-node bifurcations [1–5], which enable earlier sudden transitions before the key parameter reaches the critical value, which trigger deterministic bifurcations. Such properties of noise-induced bifurcations are strongly relevant for a broad range of scientific efforts which encounter the saddle-node. For example, the effective utilization of Josephson junction circuits to amplify minute changes in current level is dependent on various measurement noise effects [6–10] and switching-based employment of mechanical micro-/nano-mechanical oscillators requires careful understanding of stochastic sensitivities for reliable operation [11–13]. In life and biological sciences, systems characterized as exhibiting saddle-node-type phenomena reveal similar sensitivities to stochastic perturbations. This has been demonstrated for neural action potential dynamics [14–16], noise-activated escapes from ecological equilibria [17–19], and climate balance and tipping estimation [20–22].

While noise alone may prematurely induce a bifurcation, non-stationarity of the governing parameters may delay it [23–26]. When the system parameter varies at a finite rate through the critical value corresponding to adiabatic bifurcation, the actual transition may occur after the parameter passes through the adiabatic value. As a result, the system may remain at or near the original state instead of immediately undergoing the large qualitative shift in behavior, which is described to be a type of memory effect [27,28]. Delayed (also termed deferred) bifurcation phenomena have drawn special attention in laser turn-on dynamics related to the pitchfork bifurcation [27,29,30]. Delayed saddle-node bifurcations have been observed in various contexts such as in chemical reactions [31–33] and in tribological processes where they denote the influence of stick slip [34–36]. Qubit readouts for quantum computing are also subject to delayed saddle-node bifurcation which is a critical factor to understand for the useful implementation of such technologies [9,37].

Recently, great attention has been devoted to the development of robust and sensitive microscale bifurcation-based sensors due to the ease of activating strongly nonlinear behaviors on such a length scale, including the pitchfork [38–40] and saddle-node bifurcations [41–44]. By leveraging unmistakable and sudden variations in sensor behavior due to subtle perturbations to the system which induce the bifurcation, the bifurcation-based sensing methods yield significantly enhanced resolution and sensitivity compared to conventional, linear dynamics-based detection methods. To introduce these novel and high performance detection principles into the context of meso-/macro-scale mechanical and civil structural health and condition monitoring, the authors recently integrated double-well Duffing circuits with the monitored systems [45,46]. In this way, small changes in the (assumed) linear dynamics of the monitored structures may activate more dramatic shifts in the circuit behaviors, providing a robust and sensitive framework for structural monitoring. For all scales of bifurcation-based sensing, noise and non-stationary influences are

[1]Corresponding author.

Contributed by the Design Engineering Division of ASME for publication in the Journal of Computational and Nonlinear Dynamics. Manuscript received February 3, 2016; final manuscript received June 28, 2016; published online September 1, 2016. Assoc. Editor: Hiroshi Yabuno.

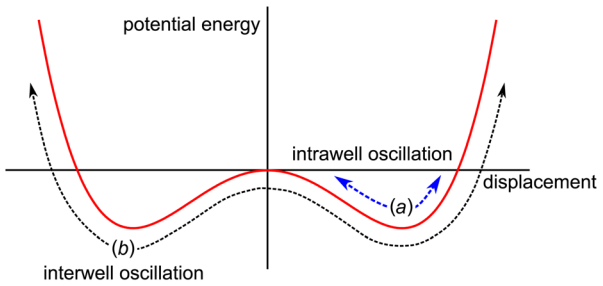

Fig. 1 Potential energy of a double-well Duffing oscillator (solid curve). Illustrative dynamic trajectories for (*a*) intrawell and (*b*) interwell steady-state oscillations.

oftentimes unavoidable, and the viability and effectiveness of these detection principles are critically tied to an understanding of the coupled, adverse phenomena.

To exemplify the importance of simultaneously taking into account the influences of non-determinism and non-stationarity on saddle-node bifurcation, the following representative experimental results are provided which leverage the saddle-node invested in a double-well Duffing analog circuit oscillator. The double-well Duffing oscillator is considered here since a dynamic saddle-node bifurcation occurs as the excitation amplitude increases while the excitation frequency is fixed below the linear resonance frequency. As a result, the steady-state intrawell oscillations confined to one of the wells of potential energy suddenly transition to interwell dynamics that span both potential wells [47–49], as illustrated in Fig. 1. Moreover, it is the double-well Duffing analog circuit that has been recently utilized as a bifurcation-based sensing device for detecting structural changes and damage in macroscale structures [45,46]. Thus, the analysis on stochastic and dynamic activation of the bifurcation directly provides an important means of characterizing the dynamics of practical bifurcation-based sensor platform. These bifurcations of the double-well Duffing oscillator may be activated either by variation in the harmonic excitation frequency using an appropriate amplitude of excitation or by variation in the excitation amplitude using an appropriate excitation frequency; in this work, the latter method is employed. Complete details on the experimental circuit fabrication and its faithful reconstruction of double-well Duffing oscillator characteristics are given in Sec. 2.

In these first experiments, the input voltage to the circuit is prescribed to be a 500 Hz sinusoid that steadily increases in amplitude from 0.3 V to 0.35 V which was identified to be an excitation form and amplitude range capable of activating the saddle-node bifurcation that demarcates the intrawell and interwell oscillation regimes. Various rates of sweeping the input voltage amplitude are employed. In addition, several intensities of Gaussian white noise are added to the input signal. This combined harmonic and stochastic input voltage excites the circuit and the mean harmonic amplitudes of circuit output voltage for 100 experimental trials are plotted according to the input voltage amplitude in Fig. 2. When the excitation is effectively a pure harmonic signal, the comparison of output voltage amplitudes in Fig. 2(*a*) shows the influence of changing the input voltage sweep rate from quasi-static conditions to a rate of 2.5 V/s. As observed in Fig. 2(*a*) by the sudden increase in the output voltage, the saddle-node bifurcation is triggered at a quasi-statically varied harmonic input voltage amplitude of approximately 0.328 V. Note that although an escaping phenomenon is shown in Fig. 2(*a*), experimentally the dynamics thereafter transition to a still higher output voltage amplitude which is characteristic of the interwell vibrations. In contrast to the quasi-static finding, as the sweep rate becomes positive and finite, the activation of the saddle-node bifurcation becomes delayed such that greater input voltage amplitude is needed to induce the event. When the sweep rate is 2.5 V/s, the activation of the bifurcation occurs at input voltage amplitude of 0.341 V.

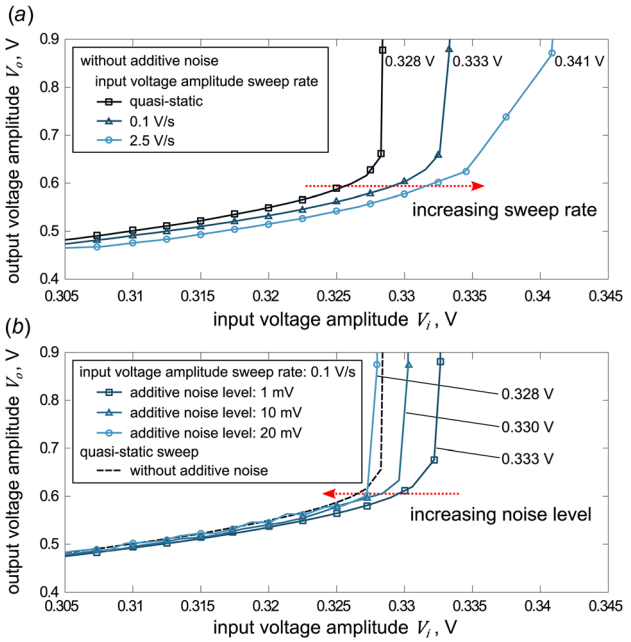

Fig. 2 Experimentally measured output voltage amplitudes of the circuit (*a*) as input voltage amplitude sweep rate varies and (*b*) in the presence of different levels of additive Gaussian white noise with a fixed sweep rate of 0.1 V/s. The critical input voltage amplitudes that activate bifurcations are presented for each case.

In other words, a delay of 4% with respect to the quasi-static bifurcation condition is induced by the non-stationary variation in the input voltage amplitude.

To exemplify the role of stochastic fluctuations in the input voltage amplitude, Fig. 2(*b*) presents the measurements when the input voltage amplitude is corrupted using various levels of additive white noise; here, the input voltage amplitude is swept at a finite rate of 0.1 V/s. The measurements in Fig. 2(*b*) clearly show that the stochastic fluctuations may induce either premature or delayed activation of the saddle-node escape. It is seen that for finite sweeping rate and low noise, a delayed activation occurs, whereas increased noise intensity may cause the bifurcation to occur prematurely using the same sweeping rate. Collectively, these results illustrate the severe sensitivities of activating the saddle-node bifurcation in the presence of non-stationary and non-deterministic excitations. Therefore, it is critical to accurately characterize the parameters which are more likely to induce the saddle-node bifurcation by directly accounting for attendant noise levels and parameter sweep rates. Without this understanding, the true approach and triggering of a saddle-node bifurcation may be incorrectly predicted, which could compromise the application such as a bifurcation-based sensing scheme or a model of ecological balance.

A number of researchers have explored the adverse coupling of non-stationary and non-deterministic influences on the activation of the saddle-node bifurcations by introducing scaling laws [50–52] and by analytically and numerically integrating the associated Fokker–Plank equation of the stochastic normal form [53]. Recently, the distribution of the escape events induced by saddle-node bifurcations has been approximately derived and numerically validated by Miller and Shaw [54]. On the other hand, this advancement requires an updated, intricate computation of the mean escape time in consequence to each change in the non-stationary and non-deterministic parameters. As a result, the computation of such statistics may become considerably involved and expensive. To overcome the limitation, this research derives a new approximate solution strategy to determine the escape statistics of non-stationary and non-deterministic activation of

saddle-node bifurcations. By validating the approach with experimental results obtained using a double-well Duffing analog circuit, the findings of this research exemplify that the approximate analytical solution provides a straightforward method to estimate the stochastic and non-stationary activation of the delayed saddle-node bifurcations.

The following sections present investigations that accomplish these goals through a collection of theoretical and experimental efforts. First, the experimental circuit is described in detail in Sec. 2, and it is shown that the circuit is faithfully modeled using the conventional governing equation form of the classical double-well Duffing oscillator which exhibits dynamic saddle-node bifurcations. In Sec. 3, the stochastic normal form of dynamic saddle-node bifurcation for the oscillator is derived to characterize the system dynamics on the slow center manifold. Using this formulation, the approximate mean escape time is derived to serve as a predictive tool for the many applications and studies for which non-stationary and stochastic triggering of the saddle-node bifurcations are crucial factors. Sec. 4 provides numerical and experimental investigations using the double-well Duffing circuit to verify the accuracy of the analytical predictions in estimating the input voltage amplitude that activates the saddle-node bifurcation for single-frequency excitations.

2 Experimental Double-Well Duffing Analog Circuit Oscillator

A schematic of the experimentally fabricated double-well Duffing analog circuit oscillator is shown in Fig. 3(*a*). The static and dynamic bistability of the circuit are facilitated by the nonlinear feedback loop among the idealized op-amp and diodes. By applying Kirchhoff's laws, the governing equation for the circuit is derived to be

$$LC\ddot{V}_o + RC\dot{V}_o + F_{\text{cir}}(V_o) = V_i(t) \tag{1}$$

where L, C, R, and F_{cir} represent the circuit inductance, capacitance, resistance, and a nonlinear voltage function, respectively; $V_i(t)$ and $V_o(t)$, respectively, indicate the input voltage of the oscillator circuit and the output voltage which exhibits bistability; and the overdot indicates the time derivative. Note that the output voltage is the generalized displacement of the oscillator circuit in Eq. (1). To derive Eq. (1) for the double-well Duffing analog circuit shown in Fig. 3(*a*), it is assumed that $R_3 \gg \sqrt{L/C}$, which is a condition satisfied experimentally. Here, the op-amp is a LM741CN while the diodes are 1N4148. The other relevant circuit parameters are given in Table 1.

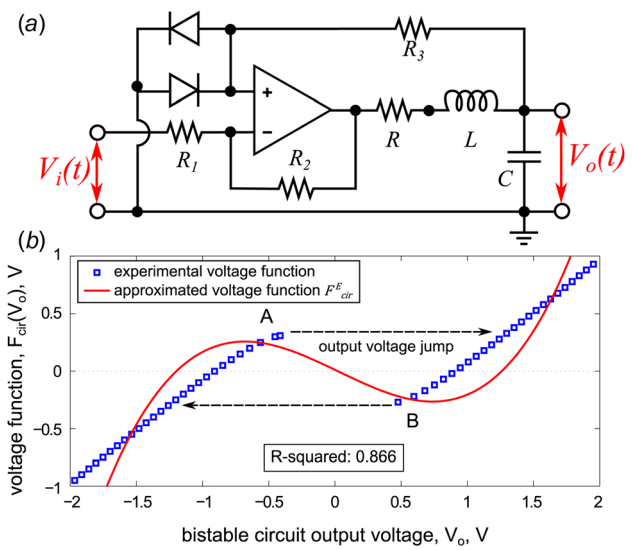

Fig. 3 (*a*) Analog circuit diagram employed in the theoretical and experimental investigation. (*b*) Experimentally measured (squares) nonlinear voltage function with respect to output voltage amplitude. The cubic polynomial fit (solid curve) has R^2 fitness of 0.866.

The qualitative piecewise-linear characteristics of the nonlinear voltage function $F_{\text{cir}}(V_o)$ verify the close similarity of the analog circuit to the conventional double-well Duffing oscillator which has a restoring force expressed by a cubic polynomial composed using negative linear and positive cubic terms [48,55,56]. The voltage function is determined by measuring the output voltage V_o as a DC input voltage $V_{i,\text{DC}}$ is quasi-statically varied within the range that encompasses the two local minima of potential energy. Thus, by Eq. (1), the quasi-static variation of the DC input voltage by $V_{i,\text{DC}}$ is equal to the voltage function: $V_{i,\text{DC}} = F_{\text{cir}}(V_o)$. Figure 3(*b*) illustrates the experimentally measured nonlinear voltage function $F_{\text{cir}}(V_o)$ with respect to the output voltage V_o. Starting from large negative values, when the DC input voltage is quasi-statically increased beyond 0.32 V, denoted as point A in Fig. 3(*b*), the output voltage V_o undergoes a sudden transition from approximately -0.36 V to $+1.30$ V. Then, as the voltage function is reduced in value (by quasi-statically reducing the DC input voltage), the bifurcation is activated at point B. By minimizing the squared difference between the analytically estimated mean escape time (detailed in Sec. 3.2) and the experimentally measured escape time, a cubic polynomial fit is obtained to approximate the nonlinear voltage function using

$$F^E_{\text{cir}}(V_o) = -a^E V_o + b^E V_o^3 \tag{2}$$

where $a^E = 0.552$ and $b^E = 0.365$. Figure 3(*b*) shows the polynomial fit (solid curve) to the experimental measurements of the voltage function (square points). The range of output voltages shown in Fig. 3(*b*) accounted for in the fitting procedure, the polynomial fit realizes a high R^2 value of 86.6% which means the fit effectively emulates the global characteristics of the exact voltage function. In addition, the critical amplitude of the voltage function amplitude that experimentally triggers the quasi-static bifurcations, ~0.32 V, is closely reconstructed by the polynomial fit, ~0.33 V. Then, by substituting Eq. (2) into Eq. (1) and rescaling parameters, the governing equation for the circuit output voltage becomes

$$\ddot{x} + 2\zeta^E\dot{x} - K^E x + G^E x^3 = P^E(t) \tag{3}$$

$$x(t) = V_o(t) \tag{3a}$$

$$\zeta^E = \frac{R}{2L} \tag{3b}$$

$$K^E = \frac{a^E}{LC} \tag{3c}$$

$$G^E = \frac{b^E}{LC} \tag{3d}$$

$$P^E(t) = \frac{V_i(t)}{LC} \tag{3e}$$

Equation (3) is evidently in the conventional form of the governing equation for the double-well Duffing oscillator where

Table 1 Experimental system parameters of the double-well Duffing circuit

L (mH)	C (μF)	R (Ω)	R_1 (kΩ)	R_2 (kΩ)	R_3 (kΩ)
10.24	0.96	82	9.07	9.08	10

the conservative restoring forces include terms having negative linear and positive cubic powers of the generalized coordinate x [47–49]. This analytical foundation verifies that the experimental circuit platform faithfully reconstructs the relevant dynamic saddle-node bifurcation phenomena exhibited by such Duffing oscillators.

3 Theoretical Analysis on the Saddle-Node Bifurcation

3.1 Stochastic Saddle-Node Bifurcation Normal Form. To investigate the non-deterministic and non-stationary influences on the activation of saddle-node bifurcations, the stochastic normal form of the saddle-node bifurcation can be derived from the double-well Duffing oscillator governing equation as (see the Appendix for derivation)

$$\dot{x} = \mu + mx^2 + D\xi \tag{4}$$

where ξ is Gaussian white noise with autocorrelation $\langle \xi(t)\xi(\tilde{t})\rangle = 2\delta(t-\tilde{t})$ and D is the effective noise strength. By scaling the variable with $y = mx$, the stochastic normal form for the steady-state saddle-node bifurcation of the double-well Duffing oscillator is found to be

$$\dot{y} = \eta + y^2 + \varepsilon\xi \tag{5}$$

with the bifurcation parameter $\eta = m\mu$ and noise strength $\varepsilon = mD$. When the parameter $\eta < 0$ quasi-statically increases, the system becomes unstable as the saddle-node bifurcation occurs at $\eta = 0$ annihilating the fixed points $y = \pm\sqrt{-\eta}$. Thus, the non-stationary influence on the saddle-node bifurcation can be assessed by examining the system stability with respect to a time-dependent bifurcation parameter $\eta(t)$. For a common case of broad practical importance, the parameter sweep rate is assumed to be constant such that

$$\eta(t) = \eta_0 + rt \tag{6}$$

The bifurcation parameter is swept from $\eta_0 < 0$ at a sweep rate of $r > 0$, which is ultimately related to the excitation amplitude P variation through the transformations and relations given in the Appendix. By substituting Eq. (6) into Eq. (5), the non-stationary and non-deterministic influences on the activation of saddle-node bifurcations can be investigated in terms of both the bifurcation parameter sweep rate and the additive noise level. Since the bifurcation parameter $\eta(t)$ varies linearly in time, the time can be scaled according to the rate of parameter change. New variables are introduced [57]

$$\tau = \eta r^{-2/3} \tag{7a}$$

$$z = yr^{-1/3} \tag{7b}$$

and substituted into Eq. (5) to yield

$$z' = \tau + z^2 + \alpha\xi \tag{8a}$$

$$\alpha = \varepsilon/r^{2/3} \tag{8b}$$

where $()'$ indicates differentiation with respect to scaled time τ. As a result, the stochastic and non-stationary influences on the activation of saddle-node bifurcation may be investigated using a single parameter, scaled noise α in Eq. (8).

3.2 Analytical Approximation of the Dynamic Saddle-Node Bifurcation. In this research, a new approximate solution strategy is developed to estimate the escape statistics of the stochastic and non-stationary activation of saddle-node bifurcations. First, the probability density of the escape events is derived from the stochastic normal form of Eq. (8). By employing the approach recently introduced by Miller and Shaw [54], the approximate PDF of the escape time T is obtained

$$P_\infty(T) = \frac{1}{\sqrt{4\pi^5\alpha^2 B_i^4(-T)\int_{-\infty}^{T} A_i^4(-\tau)d\tau}} \times \exp\left[-\frac{A_i^2(-T)/B_i^2(-T)}{4\pi^2\alpha^2\int_{-\infty}^{T} A_i^4(-\tau)d\tau}\right] \tag{9}$$

where A_i, B_i are the standard Airy functions. Since the bifurcation parameter τ, rescaled as the *time* according to Eq. (7*a*), is forward and linearly swept, the escape time T is defined to be the time at which the dynamic saddle-node bifurcation is activated as the system loses stability. In other words, the escape time T is when the response of Eq. (8) becomes unbounded such that $z \to \infty$. The PDF in Eq. (9) is subject to the constraints $\alpha \ll 1$ and $1.17 < \tau < 3.27$ [54]. For example, when $\alpha = 0.1$, the mean value of the escape time $\langle T\rangle$ is obtained by numerically integrating the PDF in Eq. (9) to be approximately 2.33. In this way, the mean escape time $\langle T\rangle$ for every different case is taken by numerically solving Eq. (9) for the corresponding scaled noise level α, which encompasses the stochastic and non-stationary parametric changes.

Then, using this previously developed foundation, the first step toward a new derivation for the mean escape time is to approximate the PDF in Eq. (9) as a Gaussian distribution. Since the system is subjected to additive Gaussian white noise perturbations, the probability density of the escape time as shown in Fig. 4 is comparable to a Gaussian. As a result, Eq. (9) is then approximated to be Gaussian using

$$P_\infty(T) \approx \frac{1}{\sqrt{2\pi}\sigma_T}\exp\left[-\frac{k_e(T-\mu_T)^2}{2\sigma_T^2}\right]\frac{1}{\pi B_i^2(-T)} \tag{10a}$$

$$\sigma_T^2 = 2\pi^2\alpha^2\int_{-\infty}^{T} A_i^4(-t)dt \tag{10b}$$

where μ_T, σ_T, and k_e are the approximate mean and standard deviation of the escape time, and the scaling coefficient, respectively. The exponential numerator in Eq. (9), denoted as $F(T)$, is approximated by a quadratic polynomial fit in Eq. (11) [58], and is plotted in Fig. 5 in comparison to the actual numerator

$$F(T) = \left(\frac{A_i(-T)}{B_i(-T)}\right)^2 \approx \tan^2\left(\frac{2}{3}T^{3/2} + \frac{\pi}{4}\right) \approx k_e(T-\mu_T)^2 \tag{11}$$

To determine μ_T, the minimum of the approximate $F(T)$ is derived, from which the mean value μ_T is computed

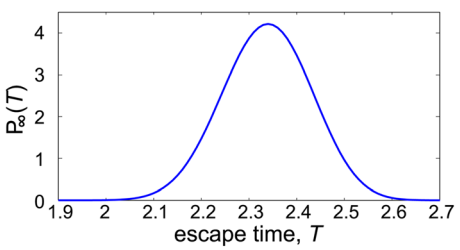

Fig. 4 Probability density of escape time T when $\alpha = 0.1$

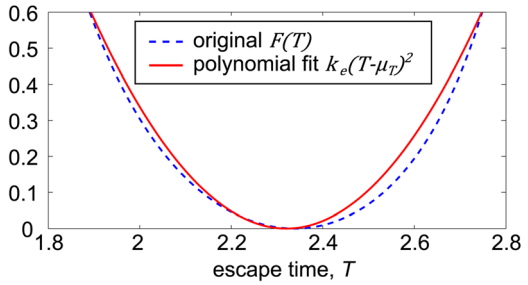

Fig. 5 The polynomial fit $k_e(T-\mu_T)^2$ (solid) of $F(T)$ (dotted curve)

$$\left.\frac{dF}{dT}\right|_{\mu_T} \approx 2\mu_T^{1/2}\tan\left(\frac{2}{3}\mu_T^{3/2}+\frac{\pi}{4}\right)\left[\tan^2\left(\frac{2}{3}\mu_T^{3/2}+\frac{\pi}{4}\right)+1\right]=0 \tag{12a}$$

$$\mu_T=\left(\frac{9\pi}{8}\right)^{2/3} \tag{12b}$$

Therefore, the mean escape time of the delayed saddle-node bifurcation can be accurately and simply obtained as μ_T for $\alpha \ll 1$ instead of numerically solving the PDF in Eq. (9) for every scaled noise level. The total processing time, for example, required more than 3 h to numerically solve the PDF and obtain the mean escape time for 100 different sweep rates (0.005–50 V/s) and noise levels (0.01–100 mV), respectively. The simulations were conducted on a standard personal computer, with an Intel Core 3.4 GHz and 16 GB of RAM. On the other hand, the mean escape time can be immediately obtained by the proposed analytical approximation (Eq. (12*b*)).

Since the bifurcation parameter is swept linearly in time, the critical parameter value that activates the bifurcation is directly related to the escape time. For prescribed noise level and parameter sweep rate, the escape excitation amplitude P_{esc}, which activates the saddle-node bifurcation, can be determined from the escape time T by a series of substitutions into the above derived expressions. For example, the actual escape time t_{esc} is obtained from the scaled escape time T by substituting Eq. (6) into Eq. (7*a*) such that $t_{\text{esc}}=1/r(Tr^{2/3}-\eta_0)$. The escape bifurcation parameter η_{esc} from Eq. (6) at time t_{esc} is scaled to $\mu_{\text{esc}}=\eta_{\text{esc}}/m$ and substituted into Eq. (A5*b*) to yield the escape excitation amplitude $P_{\text{esc}}=P_{\text{cr}}+2\zeta/m(\eta_0+rt_{\text{esc}})$. By substituting t_{esc} into P_{esc}, it is found that

$$P_{\text{esc}}=P_{\text{cr}}+\frac{2\zeta}{m}Tr^{2/3} \tag{13}$$

As a result, an accurate estimation of the mean escape excitation amplitude $\langle P_{\text{esc}}\rangle$ can be obtained by utilizing the analytical approximation of mean escape time μ_T in Eq. (12*b*).

In summary, the key result is that instead of numerically integrating Eq. (9) to obtain the mean of escape time $\langle T\rangle$ for each noise strength α, the mean escape time for the delayed saddle-node bifurcation may be more straightforwardly obtained using Eq. (12*b*). By straightforward back-calculation, the mean escape time can be used to determine the expected value of the escape excitation amplitude in Eq. (13). This escape amplitude is therefore a meaningful criterion related to the stochastic and dynamic saddle-node bifurcation in the double-well Duffing oscillator. Thus, the analytical approximation can serve as a simple tool for estimating the escape events. It is worth summarizing and commenting upon the assumptions employed to arrive at this new analytical approximation of the mean escape time: (i) small scaled noise α ; (ii) weakly damped Duffing oscillator; (iii) Gaussian white noise as stochastic influence; (iv) linearly swept bifurcation parameter. Since the standard deviation of the escape events distribution decreases and the escape events are predominantly distributed near the mean value for small scaled noise α [57], the mean escape time can effectively represent the escape time distribution and becomes the significant guide toward assessing escape events. As a result, this research is focused on estimating the mean escape time. Additionally, the inclusion of the noise leads to an effective series of random "initial conditions" for this nonlinear system, which reduces the importance of accounting for initial conditions toward predicting the saddle-node bifurcation events [54]. The concise analytical prediction of the mean escape time and the current employment of the above assumptions to arrive at this theoretical tool are validated through numerical and experimental investigations in Sec. 4.

4 Statistics of Non-deterministic and Non-stationary Activation of the Saddle-Node Bifurcation

The accuracy of the analytical approximation of mean escape time is assessed using experimental and numerical efforts. The experimental investigation is conducted by employing the double-well Duffing analog circuit introduced in Sec. 2. The double-well Duffing analog circuit is harmonically excited at 500 Hz and the input voltage amplitude is increased by sweeping across the bifurcation point starting from 0.3 V to 0.35 V. In addition to the ambient noise level, three different levels of Gaussian white noise are added to the excitation input voltage to examine the stochastic influences on the saddle-node activation. The root mean square (RMS) amplitude of the ambient noise in the experiment is 0.015 mV. The input voltage amplitude sweep rates and the additive noise levels applied in the experiment are given in Table 2. Each condition with various sweep rates and noise levels is considered 100 times. The escape input voltage amplitude V_{esc} that activates dynamic saddle-node bifurcation is recorded and utilized to determine the escape time $t_{\text{esc}}=(V_{\text{esc}}-V_0)/s_V$, where s_V is the input voltage sweep rate. The escape time is then substituted into Eq. (13) to yield the scaled escape time T.

For the numerical evaluation, the mean escape time $\langle T\rangle$ is obtained by numerically solving the PDF in Eq. (9). In addition, a Monte-Carlo-based solution of the mean escape time is obtained by solving the stochastic normal form in Eq. (8*a*) using the Euler–Maruyama method [59] 1000 times and taking the mean of the resulting escape time values. For both numerical solution

Table 2 The scaled noise level α for each input voltage amplitude sweep rate and additive noise level (RMS amplitude) applied in the experiment to examine the stochastic dynamic bifurcation in the double-well Duffing circuit

		Sweep rate (V/s)						
		0.05	0.1	0.25	0.5	1	2.5	5
Noise level (mV)	0.015	0.0521	0.0328	0.0178	0.0112	0.0071	0.0038	0.0024
	1	3.47	2.19	1.19	0.748	0.471	0.256	0.161
	10	34.7	21.9	11.9	7.48	4.71	2.56	1.61
	20	69.4	43.8	23.8	15.0	9.43	5.12	3.22

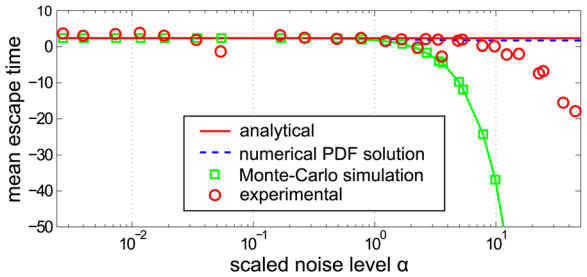

Fig. 6 The analytical approximation (solid curve) of the mean escape time is presented with the results obtained by numerically solving the PDF (dashed curve), Monte-Carlo simulation (square), and experimental measurement (circle) with respect to the scaled noise level α

forms, the computation is conducted for each scaled noise level α given in Table 2.

Figure 6 compares the new approximated solution (solid curve) of the mean escape time with those obtained by numerically solving the PDF in Eq. (9) (dashed curve), the Monte-Carlo simulation (square), and experimental measurements (circle) as a function of scaled noise level α. It can be observed that the approximated mean escape time is comparable to the numerically and experimentally obtained mean escape time distributions for small α, which represents a low level of stochastic excitation compared to the bifurcation parameter sweep rate. Stated more concretely, when the parameter is swept relatively quickly toward the bifurcation point compared to the low level of noise perturbations, the system evolves correspondingly quickly such that the basin of attraction is more likely to disappear before the noise has opportunity to prematurely activate the bifurcation. As a result, the saddle-node bifurcation is likely to be delayed in this case of small α, and the escape time becomes fairly insensitive to the low level of noise. On the other hand, the analytic prediction deviates from the numerical and experimental results when the scaled noise level is high. This error may stem from the large level of noise that violates the assumption of small perturbation near the bifurcation point to maintain the normal form valid. Therefore, the analytical approximation of the mean escape time as a constant is strongly justified under such conditions.

Figure 7 provides a comparison of two representative examples that demonstrate the high accuracy of the analytical escape time prediction with respect to acquired experimental and numerical data. In order to numerically reconstruct the voltage response of the circuit from the normal form of the saddle-node bifurcation, the amplitude $z(\tau)$ is first obtained by solving Eq. (8*a*) using the Euler–Maruyama method. Substituting $z(\tau)$ into Eq. (7*b*) and applying the scaling $y = mx$ yields $x(\tau) = (1/m)r^{1/3}z(\tau)$. The output voltage $V_o(\tau) = c^*_{\text{cr}} + a(\tau)\cos\omega\tau$ is then obtained by applying a coordinate transform $a(\tau) = a^*_{\text{cr}} + x(\tau)$ and substituting it into Eq. (A2). For the numerical reconstructions, a negative value of c^*_{cr} is selected to reflect the corresponding experimental measurements which initially oscillate around the negative-valued static equilibrium in the examples shown in Fig. 7. In this figure, the numerically simulated output voltages (dashed curves) of the circuit are plotted as a function of the input voltage amplitude and compared with the experimental measurement (solid curves) of the circuit response. Finally, the analytically determined mean escape input voltage amplitudes $\langle V_{\text{esc}}\rangle$ are plotted as dotted vertical lines in Fig. 7. The analytical prediction of the mean escape time μ_T in Eq. (12*b*) is applied to Eq. (13) assuming $\mu_T \approx \langle T\rangle$, which yields the mean escape input voltage amplitude $\langle V_{\text{esc}}\rangle$ dimensionalized via Eq. (3*e*).

Figure 7(*a*) presents the output voltage of the circuit for a case when the input voltage amplitude is swept at a rate of 0.1 V/s without additive noise; here, the ambient noise level is 0.015 mV

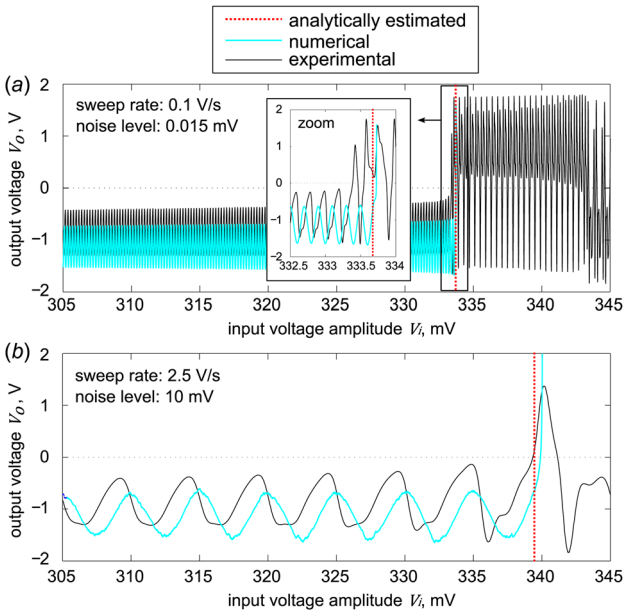

Fig. 7 Comparison of analytical, numerical, and experimental results of activating the dynamic saddle-node bifurcation of the double-well Duffing circuit. For (*a*) the input voltage amplitude is swept at rate of 0.1 V/s with 0.015 mV additive noise level, while for (*b*) the sweep rate is 2.5 V/s using 10 mV level noise. Analytically estimated mean escape input voltage amplitude $\langle V_{\text{esc}}\rangle$ for both cases is presented as dotted vertical lines.

which is negligible with respect to the harmonic excitation component. Figure 7(*b*) compares the analytical, numerical, and experimental results when the input voltage amplitude is increased at a faster rate of 2.5 V/s in the presence of a greater additive noise level, 10 mV. For both representative examples in Fig. 7, the output voltage of the double-well Duffing circuit initially exhibits intrawell oscillations around a static equilibrium; as the saddle-node bifurcation is activated, one or more interwell oscillations are induced. It is seen that the bifurcation activation is delayed from approximately 334 mV to 339 mV when the input voltage amplitude sweep rate is increased from 0.1 V/s to 2.5 V/s, seen comparing Figs. 7(*a*) and 7(*b*), respectively. Importantly, it is seen that the analytical approximation is in strong agreement with the experimental and numerical data, even for these two very different cases of sweep rate and additive noise.

For a comprehensive evaluation of the analytical method accuracy with respect to the experimental data, the mean escape input voltage amplitude $\langle V_{\text{esc}}\rangle$ that induces the dynamic saddle-node bifurcation is analytically estimated for a broad range of parameter sweep and noise conditions, as detailed in Table 2. Then, Fig. 8 plots all of the results comparing the predicted mean escape excitation voltage amplitudes as a function of the inverse of the scaled noise strength $1/\alpha$ for a variety of additive noise levels. The analytical predictions are given by dotted curves whereas the experimental results are the circle data points connected with solid curves. Each experimental data point is the mean of 100 experimental trials. As shown in Fig. 8, as the input voltage amplitude sweep rate increases, the activation of the saddle-node bifurcation is consistently delayed; this is evident from the increase in the escape voltage amplitude for increasing sweep rate. Also, the mean escape input voltage amplitudes decrease in consequence to the noise-activated escape that results from the increase in noise level. Figure 8 illustrates that the analytical approach accurately predicts the mean escape input voltage amplitudes that are observed experimentally, particularly for smaller additive noise levels (greater inverse scaled noise levels $1/\alpha$). It is seen that the analytical

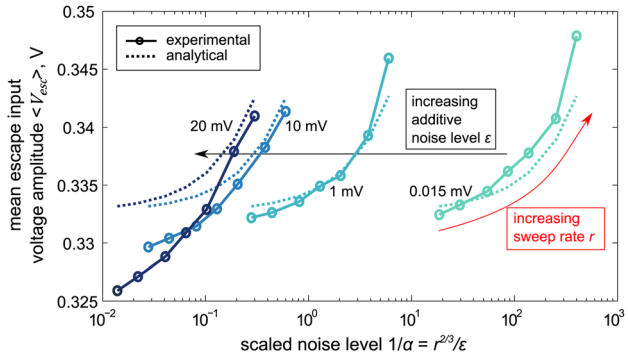

Fig. 8 Experimentally measured (data points with solid curves) and analytically estimated (dotted curves) mean escape input voltage amplitudes are presented with respect to the inverse of the scaled noise level α for each different additive noise level given next to each curve

prediction error develops at greater levels of noise and slower sweep rates. The source of such error may be the assumption of small perturbations from the dynamic steady-state in the normal form formulation, which is potentially in conflict with the large degree of deviations induced due to the greater noise near the saddle-node. Nevertheless, the analytical estimates still achieve good agreement at high levels of noise when the sweep rate increases. Overall, the accuracy of the analytical approach across such a wide range of bifurcation parameter sweep rates and noise levels supports and validates the analytical approximation given by Eq. (12*b*). By such a straightforward relation and simple series of back-calculations to predict and determine parameters to induce escape, the analytical approximation derived herein provides a valuable new means for predicting the onset of saddle-node bifurcation under the non-stationary and non-deterministic conditions common to a variety of contexts.

5 Conclusion

The non-stationary and stochastic influences on the activation of saddle-node bifurcation are investigated to develop a new analytical prediction strategy for critical parameters that induce escape from a stable equilibrium. The double-well Duffing oscillator serves as the archetypal system of interest due to its ability to exhibit a dynamic saddle-node bifurcation. The stochastic normal form of the saddle-node bifurcation is derived from the governing equation of the oscillator and is utilized to formulate the escape probability density. A new, concise approximation of the mean escape time is formulated, yielding straightforward and effective means to predict the escape excitation amplitude that activates the bifurcation. Numerical and experimental investigations conducted using a double-well Duffing analog circuit verify the accuracy of the analytical approximation. The findings moreover exemplify the critical roles of non-stationarity and non-determinism on the activation of the saddle-node bifurcation. Based upon the broad applicability and relevance of saddle-node bifurcation phenomena across many scientific and technical disciplines, the analytical method developed here may be utilized for simple and accurate determination of critical operating environments that influence the susceptibility of the system to being pushed beyond the "tipping point" [19].

Acknowledgment

This research is supported by the National Science Foundation under Award No. 1232436 and by the University of Michigan Collegiate Professorship fund.

Appendix: Derivation of the Stochastic Normal Form of Saddle-Node Bifurcation

This appendix provides a detailed derivation of the stochastic normal form of the saddle-node bifurcation from the double-well Duffing oscillator governing equation. When the oscillator is harmonically excited, the analog circuit Eq. (3) is expressed using a comparable form

$$\ddot{X} + 2\zeta\dot{X} - KX + GX^3 = P\cos\omega t \tag{A1}$$

where $X(t)$, ζ, P, and ω are, respectively, the generalized coordinate, dissipation factor, amplitude of excitation, and excitation frequency. K and G are linear and nonlinear stiffness coefficients, respectively. In Eq. (A1), an overdot indicates a differentiation with respect to time t. Depending upon the harmonic excitation amplitude P, the steady-state response of the system may evolve from intrawell oscillations around one of the two stable equilibria $X^* = \pm\sqrt{K/G}$ to interwell oscillations, which cross the unstable equilibrium $X^* = 0$, or evolve in the opposite trend. The harmonic balance method [49,60–62] is applied to approximately represent the steady-state dynamics of Eq. (A1) for sufficiently small damping $0 < \zeta \ll 1$. As a result, the steady-state response of the oscillator is assumed as a single-term Fourier series expansion

$$X = c(t) + a(t)\cos\omega t \tag{A2}$$

The term $c(t)$ is necessary to represent the intrawell oscillation of the system. Substituting Eq. (A2) into Eq. (A1), assuming that the contribution of higher harmonics is negligible, and balancing the constant terms and the harmonic terms, the following equations are obtained:

$$2\zeta\dot{c} + Gc^3 + \frac{3}{2}Ga^2c - Kc = 0 \tag{A3a}$$

$$2\dot{a}\omega + 2\zeta a\omega = 0 \tag{A3b}$$

$$2\zeta\dot{a} - a\omega^2 - Ka + 3Gac^2 + \frac{3}{4}Ga^3 = P \tag{A3c}$$

where the fixed points of system (A3), (c^*, a^*), yield a trivial result for $a*$ via Eq. (A3*b*). Although the system exhibits two saddle-node bifurcations as the amplitude of single-frequency excitation is subsequently increased and decreased, for consistency this investigation focuses on the saddle-node bifurcation that separates the low amplitude intrawell from the high amplitude interwell dynamics which occurs for increasing amplitude of the excitation. Thus, the system is assumed to initially exhibit intrawell oscillation, which is representative of the nonzero fixed point $c^* = \pm\sqrt{(K/G) - (3/2)a^{*2}}$ found by solving Eq. (A3*a*). The sign of c^* is arbitrarily selected based upon assumption of the initial stable equilibrium around which the intrawell oscillations occur. By substituting the positive value of c^* into Eq. (A3*c*) and introducing a small perturbation, $\hat{x} = a - a^*$, the local dynamics around the fixed point a^* are described by

$$\dot{\hat{x}} = \left(\frac{\omega^2 - 2K}{2\zeta} + \frac{45}{8\zeta}Ga^{*2}\right)\hat{x} + \frac{45}{8\zeta}Ga^*\hat{x}^2 + \frac{15}{8\zeta}G\hat{x}^3 \tag{A4}$$

Since the stability of the response at the fixed point a^* is determined by the first term on the right-hand side of Eq. (A4), the saddle-node bifurcation occurs at fixed point a^*_{cr} with critical amplitude of excitation P_{cr} to induce the steady-state bifurcation

$$a^*_{cr} = \sqrt{\frac{4}{45G}(2K - \omega^2)} \tag{A5a}$$

$$P_{cr} = (2K - \omega^2)a^*_{cr} - \frac{15}{4}Ga^{*3}_{cr} \tag{A5b}$$

When Eqs. (A5*a*) and (A5*b*) are substituted into Eq. (A3*c*) and a coordinate transform, $\rho = P - P_{cr}$, is applied, the equation shifts to the origin such that the bifurcation occurs when $\rho = 0$

$$\dot{x} = \mu + mx^2 + O(x^3) \tag{A6a}$$

$$\mu = \frac{\rho}{2\zeta} \tag{A6b}$$

$$m = \frac{45}{8\zeta}Ga^*_{cr} \tag{A6c}$$

When additive white noise is assumed to work on the system (A6) and the higher order effects are neglected, we finally have the Langevin equation of the perturbed system as shown in Eq. (4).

References

[1] Hanggi, P., 1986, "Escape From a Metastable State," J. Stat. Phys., **42**(1–2), pp. 105–148.
[2] Meunier, C., and Verga, A. D., 1988, "Noise and Bifurcations," J. Stat. Phys., **50**(1–2), pp. 345–375.
[3] Dykman, M. I., Mori, E., Ross, J., and Hunt, P. M., 1994, "Large Fluctuations and Optimal Paths in Chemical Kinetics," J. Chem. Phys., **100**(8), pp. 5735–5750.
[4] Arnold, L., 1998, *Random Dynamical Systems*, Springer, Berlin, Germany.
[5] Dykman, M. I., Schwartz, I. B., and Shapiro, M., 2005, "Scaling in Activated Escape of Underdamped Systems," Phys. Rev. E, **72**(2), p. 021102.
[6] Fulton, T. A., and Dunkleberger, L. N., 1974, "Lifetime of the Zero-Voltage State in Josephson Tunnel Junctions," Phys. Rev. B, **9**(11), pp. 4760–4769.
[7] Büttiker, M., Harris, E. P., and Landauer, R., 1983, "Thermal Activation in Extremely Underdamped Josephson-Junction Circuits," Phys. Rev. B, **28**(3), pp. 1268–1275.
[8] Devoret, M. H., Esteve, D., Martinis, J. M., Cleland, A., and Clarke, J., 1987, "Resonant Activation of a Brownian Particle Out of a Potential Well: Microwave-Enhanced Escape From the Zero-Voltage State of a Josephson Junction," Phys. Rev. B, **36**(1), pp. 58–73.
[9] Vijay, R., Devoret, M. H., and Siddiqi, I., 2009, "Invited Review Article: The Josephson Bifurcation Amplifier," Rev. Sci. Instrum., **80**(11), p. 111101.
[10] Zorin, A. B., 1996, "Quantum-Limited Electrometer Based on Single Cooper Pair Tunneling," Phys. Rev. Lett., **76**(23), pp. 4408–4411.
[11] Aldridge, J. S., and Cleland, A. N., 2005, "Noise-Enabled Precision Measurements of a Duffing Nanomechanical Resonator," Phys. Rev. Lett., **94**(15), p. 156403.
[12] Badzey, R. L., Zolfagharkhani, G., Gaidarzhy, A., and Mohanty, P., 2005, "Temperature Dependence of a Nanomechanical Switch," Appl. Phys. Lett., **86**(2), p. 023106.
[13] Stambaugh, C., and Chan, H. B., 2006, "Noise-Activated Switching in a Driven Nonlinear Micromechanical Oscillator," Phys. Rev. B, **73**(17), p. 172302.
[14] Longtin, A., 1993, "Stochastic Resonance in Neuron Models," J. Stat. Phys., **70**(1–2), pp. 309–327.
[15] Lindner, B., Longtin, A., and Bulsara, A., 2003, "Analytic Expressions for Rate and CV of a Type I Neuron Driven by White Gaussian Noise," Neural Comput., **15**(8), pp. 1761–1788.
[16] Lindner, B., García-Ojalvo, J., Neiman, A., and Schimansky-Geier, L., 2004, "Effects of Noise in Excitable Systems," Phys. Rep., **392**(6), pp. 321–424.
[17] Guttal, V., and Jayaprakash, C., 2008, "Changing Skewness: An Early Warning Signal of Regime Shifts in Ecosystems," Ecol. Lett., **11**(5), pp. 450–460.
[18] Dakos, V., van Nes, E. H., D'Odorico, P., and Scheffer, M., 2012, "Robustness of Variance and Autocorrelation as Indicators of Critical Slowing Down," Ecology, **93**(2), pp. 264–271.
[19] Scheffer, M., Carpenter, S. R., Lenton, T. M., Bascompte, J., Brock, W., Dakos, V., van de Koppel, J., van de Leemput, I. A., Levin, S. A., van Nes, E. H., Pascual, M., and Vandermeer, J., 2012, "Anticipating Critical Transitions," Science, **338**(6105), pp. 344–348.
[20] Lenton, T. M., 2011, "Early Warning of Climate Tipping Points," Nat. Clim. Change, **1**(4), pp. 201–209.
[21] Thompson, J. M. T., and Sieber, J., 2011, "Predicting Climate Tipping as a Noisy Bifurcation: A Review," Int. J. Bifurcation Chaos, **21**(2), pp. 399–423.
[22] Scheffer, M., Bascompte, J., Brock, W. A., Brovkin, V., Carpenter, S. R., Dakos, V., Held, H., van Nes, E. H., Rietkerk, M., and Sugihara, G., 2009, "Early-Warning Signals for Critical Transitions," Nature, **461**(7260), pp. 53–59.
[23] Lu, C.-H., and Evan-Iwanowski, R. M., 1994, "The Nonstationary Effects on a Softening Duffing Oscillator," Mech. Res. Commun., **21**(6), pp. 555–564.
[24] Haberman, R., 1979, "Slowly Varying Jump and Transition Phenomena Associated With Algebraic Bifurcation Problems," SIAM J. Appl. Math., **37**(1), pp. 69–106.
[25] Berglund, N., and Kunz, H., 1999, "Memory Effects and Scaling Laws in Slowly Driven Systems," J. Phys. A, **32**(1), pp. 15–39.
[26] Kogan, O., 2007, "Controlling Transitions in a Duffing Oscillator by Sweeping Parameters in Time," Phys. Rev. E, **76**(3), p. 037203.
[27] Mandel, P., and Erneux, T., 1987, "The Slow Passage Through a Steady Bifurcation: Delay and Memory Effects," J. Stat. Phys., **48**(5–6), pp. 1059–1070.
[28] Baer, S. M., Erneux, T., and Rinzel, J., 1989, "The Slow Passage Through a Hopf Bifurcation: Delay, Memory Effects, and Resonance," SIAM J. Appl. Math., **49**(1), pp. 55–71.
[29] Mandel, P., and Erneux, T., 1984, "Laser Lorenz Equations With a Time-Dependent Parameter," Phys. Rev. Lett., **53**(19), pp. 1818–1820.
[30] Zeghlache, H., Mandel, P., and Van den Broeck, C., 1989, "Influence of Noise on Delayed Bifurcations," Phys. Rev. A, **40**(1), pp. 286–294.
[31] Erneux, T., and Laplante, J. P., 1989, "Jump Transition Due to a Time-Dependent Bifurcation Parameter in the Bistable Ioadate–Arsenous Acid Reaction," J. Chem. Phys., **90**(11), pp. 6129–6134.
[32] Koper, M. T. M., and Aguda, B. D., 1996, "Experimental Demonstration of Delay and Memory Effects in the Bifurcations of Nickel Electrodissolution," Phys. Rev. E, **54**(1), pp. 960–963.
[33] Koper, M. T. M., 1998, "Non-Linear Phenomena in Electrochemical Systems," J. Chem. Soc., Faraday Trans., **94**(10), pp. 1369–1378.
[34] Elmer, F. J., 1997, "Nonlinear Dynamics of Dry Friction," J. Phys. A, **30**(17), pp. 6057–6063.
[35] Sang, Y., Dubé, M., and Grant, M., 2001, "Thermal Effects on Atomic Friction," Phys. Rev. Lett., **87**(17), p. 174301.
[36] Conley, W. G., Krousgrill, C. M., and Raman, A., 2008, "Stick-Slip Motions in the Friction Force Microscope: Effects of Tip Compliance," Tribol. Lett., **29**(1), pp. 23–32.
[37] Siddiqi, I., Vijay, R., Pierre, F., Wilson, C. M., Metcalfe, M., Rigetti, C., Frunzio, L., and Devoret, M. H., 2004, "RF-Driven Josephson Bifurcation Amplifier for Quantum Measurement," Phys. Rev. Lett., **93**(20), p. 207002.
[38] Zhang, W., and Turner, K. L., 2005, "Application of Parametric Resonance Amplification in a Single-Crystal Silicon Micro-Oscillator Based Mass Sensor," Sens. Actuators, A, **122**(1), pp. 23–30.
[39] Yie, Z., Zielke, M. A., Burgner, C. B., and Turner, K. L., 2011, "Comparison of Parametric and Linear Mass Detection in the Presence of Detection Noise," J. Micromech. Microeng., **21**(2), p. 025027.
[40] Burgner, C. B., Miller, N. J., Shaw, S. W., and Turner, K. L., 2010, "Parameter Sweep Strategies for Sensing Using Bifurcations in MEMS," Solid-State Sensor, Actuator, and Microsystems Workshop, Hilton Head Island, SC, June 6–10, 2010, p. 130.
[41] Younis, M. I., and Alsaleem, F., 2009, "Exploration of New Concepts for Mass Detection in Electrostatically-Actuated Structures Based on Nonlinear Phenomena," ASME J. Comput. Nonlinear Dyn., **4**(2), p. 021010.
[42] Kumar, V., Boley, J. W., Yang, Y., Ekowaluyo, H., Miller, J. K., Chiu, G. T.-C., and Rhoads, J. F., 2011, "Bifurcation-Based Mass Sensing Using Piezoelectrically-Actuated Microcantilevers," Appl. Phys. Lett., **98**(15), p. 153510.
[43] Harne, R. L., and Wang, K. W., 2014, "A Bifurcation-Based Coupled Linear-Bistable System for Microscale Mass Sensing," J. Sound Vib., **333**(8), pp. 2241–2252.
[44] Khater, M. E., Al-Ghamdi, M., Park, S., Stewart, K. M. E., Abdel-Rahman, E. M., Penlidis, A., Nayfeh, A. H., Abdel-Aziz, A. K. S., and Basha, M., 2014, "Binary MEMS Gas Sensors," J. Micromech. Microeng., **24**(6), p. 065007.
[45] Harne, R. L., and Wang, K. W., 2013, "Robust Sensing Methodology for Detecting Change With Bistable Circuitry Dynamics Tailoring," Appl. Phys. Lett., **102**(20), p. 203506.
[46] Kim, J., Harne, R. L., and Wang, K. W., 2015, "Enhancing Structural Damage Identification Robustness to Noise and Damping With Integrated Bistable and Adaptive Piezoelectric Circuitry," ASME J. Vib. Acoust., **137**(1), p. 011003.
[47] Guckenheimer, J., and Holmes, P., 1983, *Nonlinear Oscillations, Dynamical Systems, and Bifurcations of Vector Fields*, Springer-Verlag, New York.
[48] Kovacic, I., and Brennan, M. J., 2011, *The Duffing Equation: Nonlinear Oscillators and Their Behaviour*, Wiley, Hoboken, NJ.
[49] Virgin, L. N., 2000, *Introduction to Experimental Nonlinear Dynamics: A Case Study in Mechanical Vibration*, Cambridge University Press, Cambridge, UK.
[50] Breban, R., Nusse, H. E., and Ott, E., 2003, "Scaling Properties of Saddle-Node Bifurcations on Fractal Basin Boundaries," Phys. Rev. E, **68**(6), p. 066213.
[51] Berglund, N., and Gentz, B., 2006, *Noise-Induced Phenomena in Slow-Fast Dynamical Systems: A Sample-Paths Approach*, Springer Science & Business Media, New York.
[52] Kuehn, C., 2015, *Multiple Time Scale Dynamics*, Springer, New York.
[53] Nicolis, C., and Nicolis, G., 2014, "Dynamical Responses to Time-Dependent Control Parameters in the Presence of Noise: A Normal Form Approach," Phys. Rev. E, **89**(2), p. 022903.
[54] Miller, N. J., and Shaw, S. W., 2012, "Escape Statistics for Parameter Sweeps Through Bifurcations," Phys. Rev. E, **85**(4), p. 046202.
[55] Cao, Q., Wiercigroch, M., Pavlovskaia, E. E., Thompson, J. M. T., and Grebogi, C., 2008, "Piecewise Linear Approach to an Archetypal Oscillator for Smooth and Discontinuous Dynamics," Philos. Trans. R. Soc., A, **366**(1865), pp. 635–652.
[56] Zou, K., and Nagarajaiah, S., 2015, "Study of a Piecewise Linear Dynamic System With Negative and Positive Stiffness," Commun. Nonlinear Sci. Numer. Simul., **22**(1), pp. 1084–1101.

[57] Miller, N., Burgner, C., Dykman, M., Shaw, S., and Turner, K., 2010, "Fast Estimation of Bifurcation Conditions Using Noisy Response Data," SPIE Smart Structures and Materials + Nondestructive Evaluation and Health Monitoring, San Diego, CA, Mar. 31, 2010, p. 764700.
[58] Abramowitz, M., and Stegun, I. A., eds., 1972, *Handbook of Mathematical Functions: With Formulas, Graphs, and Mathematical Tables*, Dover, New York.
[59] Higham, D. J., 2001, "An Algorithmic Introduction to Numerical Simulation of Stochastic Differential Equations," SIAM Rev., **43**(3), pp. 525–546.
[60] Mann, B. P., Barton, D. A. W., and Owens, B. A. M., 2012, "Uncertainty in Performance for Linear and Nonlinear Energy Harvesting Strategies," J. Intell. Mater. Syst. Struct., **23**(13), pp. 1451–1460.
[61] Stanton, S. C., Owens, B. A. M., and Mann, B. P., 2012, "Harmonic Balance Analysis of the Bistable Piezoelectric Inertial Generator," J. Sound Vib., **331**(15), pp. 3617–3627.
[62] Harne, R. L., Thota, M., and Wang, K. W., 2013, "Concise and High-Fidelity Predictive Criteria for Maximizing Performance and Robustness of Bistable Energy Harvesters," Appl. Phys. Lett., **102**(5), p. 053903.